ARL-TR-8242 • Dec 2017

US Army Research Laboratory

Topology Optimization for Reducing Additive Manufacturing Processing Distortions

by Raymond A Wildman and Andrew T Gaynor

Approved for public release; distribution is unlimited.

NOTICES

Disclaimers

The findings in this report are not to be construed as an official Department of the Army position unless so designated by other authorized documents.

Citation of manufacturer's or trade names does not constitute an official endorsement or approval of the use thereof.

Destroy this report when it is no longer needed. Do not return it to the originator.

ARL-TR-8242 ● Dec 2017

US Army Research Laboratory

Topology Optimization for Reducing Additive Manufacturing Processing Distortions

by Raymond A Wildman and Andrew T Gaynor
Weapons and Materials Research Directorate, ARL

Approved for public release; distribution is unlimited.

REPORT DOCUMENTATION PAGE

Form Approved
OMB No. 0704-0188

Public reporting burden for this collection of information is estimated to average 1 hour per response, including the time for reviewing instructions, searching existing data sources, gathering and maintaining the data needed, and completing and reviewing the collection information. Send comments regarding this burden estimate or any other aspect of this collection of information, including suggestions for reducing the burden, to Department of Defense, Washington Headquarters Services, Directorate for Information Operations and Reports (0704-0188), 1215 Jefferson Davis Highway, Suite 1204, Arlington, VA 22202-4302. Respondents should be aware that notwithstanding any other provision of law, no person shall be subject to any penalty for failing to comply with a collection of information if it does not display a currently valid OMB control number.

PLEASE DO NOT RETURN YOUR FORM TO THE ABOVE ADDRESS.

1. REPORT DATE *(DD-MM-YYYY)*	2. REPORT TYPE	3. DATES COVERED (From - To)
December 2017	Technical Report	October 2015-September 2017

4. TITLE AND SUBTITLE
Topology Optimization for Reducing Additive Manufacturing Processing Distortions

5a. CONTRACT NUMBER

5b. GRANT NUMBER

5c. PROGRAM ELEMENT NUMBER

6. AUTHOR(S)
Raymond A Wildman and Andrew T Gaynor

5d. PROJECT NUMBER
AH80

5e. TASK NUMBER

5f. WORK UNIT NUMBER

7. PERFORMING ORGANIZATION NAME(S) AND ADDRESS(ES)
US Army Research Laboratory
ATTN: RDRL-WMM-B
Aberdeen Proving Ground, MD 21005-5066

8. PERFORMING ORGANIZATION REPORT NUMBER
ARL-TR-8242

9. SPONSORING/MONITORING AGENCY NAME(S) AND ADDRESS(ES)

10. SPONSOR/MONITOR'S ACRONYM(S)

11. SPONSOR/MONITOR'S REPORT NUMBER(S)

12. DISTRIBUTION/AVAILABILITY STATEMENT
Approved for public release; distribution is unlimited.

13. SUPPLEMENTARY NOTES
primary author's email: <raymond.a.wildman.civ@mail.mil>.

14. ABSTRACT
A method is presented for combining topology optimization with an approximate additive manufacturing process model so as to reduce thermal distortions induced during the build process. Thermal distortions are detrimental in any manufacturing process, though in some additive manufacturing processes these distortions may cause a build to completely fail. Here, 2 approximate manufacturing models are used in conjunction with a compliance minimization topology optimization problem. First, a quasi-static thermomechanical model is used that approximates distortions induced by the cooling of the material. Second, an element birth model is used in which elements are activated in turn, and a similar quasi-static thermomechanical problem is used at each step. The overall algorithm uses a compromise objective function to weight the 2 goals: thermal displacement minimization and compliance minimization. These models are compared along with a strict overhang constraint method.

15. SUBJECT TERMS
residual stress, process model, thermal expansion, thermomechanical, optimization

16. SECURITY CLASSIFICATION OF:			17. LIMITATION OF ABSTRACT	18. NUMBER OF PAGES	19a. NAME OF RESPONSIBLE PERSON
a. REPORT	b. ABSTRACT	c. THIS PAGE			Raymond A Wildman
Unclassified	Unclassified	Unclassified	UU	32	19b. TELEPHONE NUMBER (Include area code) 410-306-2232

Standard Form 298 (Rev. 8/98)
Prescribed by ANSI Std. Z39.18

Contents

Approved for public release; distribution is unlimited.

List of Figures

List of Tables

Approved for public release; distribution is unlimited.

1. Introduction

Additive manufacturing (AM) is a production method that involves gradual, layer-by-layer building of material, rather than traditional methods such as milling material from a blank (subtractive manufacturing) or casting molten material into a mold. There are several AM methods for a wide range of materials, such as extrusion deposition, light polymerization, selective laser melting, and selective laser sintering. Each of these methods can be used with various materials such as polymers, ceramics, and metal alloys.

While AM has greatly expanded the design space—allowing the production of previously unmanufacturable topologically optimized structures—constraints remain. One constraint, for example, is simply the minimum allowable feature size of a manufacturing technique. In other words, each technique has a lower limit on the size of fine features that may be manufactured. One method of imposing a minimum feature size is to use a Heaviside projection method.[1] While the minimum feature size is a necessary constraint for any AM process (a feature size smaller than the minimum printable feature size is simply impossible), there are some constraints that impact the success rate of AM builds. One such AM constraint specifically related to powder bed methods is part failures due to overhanging material without the inclusion of sacrificial supports.[2] Powder bed method part failures typically occur because of unsupported, overhanging features that curl or warp under thermal load and are subsequently struck by the recoater blade/roller. Support structures act to wick heat away and provide structural support to prevent thermally induced curling.

One approach to correcting the overhang issue is to incorporate strict overhang constraints on the optimized geometry.[3] Alternatively, a physics-based method may be used wherein a process model is incorporated into the optimization method and some parameter of that process is optimized. Here, we attempt to minimize thermal distortions induced by the manufacturing process, which should reduce the need for sacrificial supports. Because a full-resolution process model would be too computationally expensive to use in an optimization loop, we propose 2 surrogate models for the manufacturing process. The first is a basic thermomechanical model that assumes that the built part is heated to a uniform initial temperature (T_0) and cools to a final temperature (T_f). The second is a thermomechanical element-birth model in which elements are activated sequentially, and activated elements have a given

Approved for public release; distribution is unlimited.

initial temperature. The activated elements then cool according to a given thermal history, eventually reaching a final temperature as before. This surrogate model simulates the AM process more closely because in direct metal laser sintering (and related techniques), features are birthed through the laser heat source hitting the powder, selectively melting a small section of the powder bed. This molten material then cools to solidify as a solid metallic feature within the part topology.

2. Problem Definition

In this section, overviews of the compliance minimization and the thermomechanical deformation problems are given. In each case, a finite element (FE) discretization of the underlying partial differential equations is used and will not be described in detail. Overall, the optimization problem will be to place material in a design domain denoted Ω, which is divided into a union of N cells or elements ω^e ($\cup_{e=1}^{N} \omega^e = \Omega$), which are quadrilaterals in 2-D or hexahedron in 3-D. Bilinear and trilinear basis and testing functions are used in 2-D and 3-D, respectively.

2.1 Heaviside Projection

The Heaviside projection method (HPM) for topology optimization was first introduced by Guest et al.[1] and provides explicit control over minimum length scale in addition to eliminating checkerboard solutions.[4] In the HPM (in contrast to sensitivity filtering or density filtering) the design space ($\boldsymbol{\phi}$) is separated from the physical space ($\boldsymbol{\rho}$) or mesh elements. Typically, the design variable locations are coincident with the mesh nodes in physical space, though this is often out of convenience—the design variables may exist anywhere in the domain. As will be seen, minimum length scale control is achieved by linking the physical space to the design space through a neighborhood with a specified minimum radius, r_{min}. In this way, only the design variables ϕ^i within the specified minimum length scale will contribute to the density ρ^e of element e.

More specifically, each element (which corresponds to physical variables) is assigned a local neighborhood set containing design variables, defined as

$$i \in N_L^e \quad \text{if } \|\mathbf{x}_i - \bar{\mathbf{x}}^e\| \leq r_{min}, \tag{1}$$

where $\mathbf{x}_i$ is the location of the i^{th} design variable and $\bar{\mathbf{x}}^e$ is the location of the centroid of the e^{th} element. This neighborhood is then used to define an intermediate

Approved for public release; distribution is unlimited.

variable μ^e, which is a weighted average of design variables

$$\mu^e = \frac{\sum_{i \in N_L^e} \phi^i w(\mathbf{x}_i - \bar{\mathbf{x}}^e)}{\sum_{j \in N_L^e} w(\mathbf{x}_j - \bar{\mathbf{x}}^e)}, \tag{2}$$

where weighting function w is defined as

$$w(\mathbf{x}_i - \bar{\mathbf{x}}^e) = 1 - \frac{\|\mathbf{x}_i - \bar{\mathbf{x}}^e\|}{r_{min}}. \tag{3}$$

Finally, the unpenalized physical variables $\boldsymbol{\rho}$ are defined via $\boldsymbol{\mu}$ as

$$\rho^e = H(\mu^e(\phi)) = 1 - e^{-\beta \mu^e(\boldsymbol{\phi})} + \frac{\mu^e(\boldsymbol{\phi})}{\phi_{max}} e^{-\beta \phi_{max}}, \tag{4}$$

where $H(\cdot)$ is the regularized (continuous approximation) Heaviside function and β controls the curvature of the regularization and may range from 5 to upwards of 50. Note that as β approaches infinity, the regularized (continuous) Heaviside function approaches the true discontinuous Heaviside function. While the design becomes more crisp (i.e., the width of the transition regions from $\rho^e = 1$ to $\rho^e = 0$ is reduced) as β increases, the function becomes more nonlinear, making the optimization more susceptible to suboptimal local minima.

A penalization scheme is necessary to encourage convergence to 0-1 designs that have minimal intermediate values of ρ^e. For a given elemental density ρ^e, a penalization reduces the element stiffness while leaving the density used for computing the volume fraction unchanged. This reduction in stiffness then causes intermediate densities to be inefficient. The most common penalization scheme is solid isotropic material with penalization (SIMP),[5,6] given by

$$\rho_*^e = (\rho^e)^p \left(1 - \rho_{\text{min}}\right) + \rho_{\text{min}}, \tag{5}$$

where p is a penalization exponent and ρ_{min} is a minimum density used to avoid setting the stiffness to zero.

Approved for public release; distribution is unlimited.

2.2 Compliance

For the static compliance minimization problem, the goal is to optimize the distribution of material, again denoted by $\boldsymbol{\rho}$, across the design domain so as to minimize external work subject to a volume of material constraint. Physical variable ρ^e represents the volume fraction of element e, which modifies the material properties of the element. The resulting optimization formulation takes on the following well-known form:

$$\begin{aligned} \min_{\boldsymbol{\phi}} \; & c(\boldsymbol{\phi}) = \mathbf{F}^{\mathrm{T}}\mathbf{d} \\ \text{subject to:} \quad & \mathbf{K}(\boldsymbol{\phi})\mathbf{d} = \mathbf{F} \\ & \sum_{e=1}^{N} \rho^e(\boldsymbol{\phi}) v^e \leq V \\ & 0 \leq \phi^i \leq \phi^i_{\max} = 1 \quad \forall i \in \Omega \end{aligned} \tag{6}$$

where $\mathbf{F}$ is the vector of applied nodal loads, $\mathbf{d}$ is the vector of nodal displacements, $\mathbf{K}$ is the global stiffness matrix, v^e is the volume of element e, and V is the total allowable material volume. For later use, let us also define the variable v_f as the total allowable volume fraction, or the ratio of V to the total volume of the design domain.

2.3 Approximate Process Model

A high-fidelity AM process model must consider numerous aspects that would be difficult to fully capture in an optimization algorithm. For example, selective laser melting involves a laser impinging on a powder bed and melting the powder in an area determined by powder depth, absorption, temperature, laser power, focal length, and beam width. After melting, the material solidifies and heat is transfered to the surrounding material, including both built material and powder. The heat is also transfered to the surrounding environment and build plate. While the consolidated material cools, it undergoes thermal deformation and may warp the surrounding built material. This thermal deformation is the most important aspect to capture for this study, and so we attempt to approximate this process with the surrogate models discussed below.

In both models described next, the objective function is defined as

$$d_{\text{therm}} = \sum_e \rho^e_* \|\mathbf{u}^e\|, \tag{7}$$

Approved for public release; distribution is unlimited.

where $\|\mathbf{u}^e\|$ is the magnitude of the displacement at the centroid of element e.

2.3.1 Basic Thermomechanical Model

The first approach is a basic thermomechanical surrogate model in which linear, isotropic thermal expansion is used. The optimization formulation is then modified to

$$\begin{aligned} &\min_{\boldsymbol{\phi}} d_{\text{therm}}(\boldsymbol{\phi}) \\ \text{subject to:} \quad &\mathbf{K}(\boldsymbol{\phi})\mathbf{d} = \mathbf{F}_{\text{therm}} \\ &\sum_{e=1}^{N} \rho_e(\boldsymbol{\phi}) v_e = V \end{aligned} \tag{8}$$

where $\mathbf{F}_{\text{therm}}$ are thermal loads induced by the thermal stress (defined by thermal expansion coefficient α and temperature difference ΔT) and the bounds on $\boldsymbol{\phi}$ are also constrained as before. Note that the total volume constraint is now an equality constraint, though this may be relaxed when the 2 optimization problems are combined into a compromise objective function. The build plate is modeled as a fixed displacement boundary condition along one edge of the design domain and is distinct from the boundary conditions applied in the compliance minimization problem described above. This approach is similar to that of Reference 7, though the thermomechanical problem is solved separately, with different boundary conditions.

2.3.2 Element Birth Model

The element birth model involves the iterative activation of elements in an FE mesh to simulate the AM-like process of adding solid material to a structure. In this model, the physics involved remains purely thermomechanical, though the iterative placement of material changes the overall deformation of the resulting structure. As such, no thermal diffusion is used, though it will be added in the future. Instead, a linear temperature history is assumed for each element, starting at T_0 and decreasing by an amount ΔT at each step. This temperature history is an oversimplification of the process and only used here for simplicity. In general, the temperature profile of an element should be measured experimentally and will not be a simple linear function of time.

Figure 1 illustrates the element activation process and per-element temperature histories. First, all elements are initialized as inactive. An inactive element has its

Approved for public release; distribution is unlimited.

Young's modulus E set to a low value E_{min} and its thermal expansion coefficient α set to zero. Next, the first element (or set of elements) is activated and its temperature reduced by ΔT and the thermal deformation of the entire mesh is computed. Note that when elements (other than the first) are activated, they may exhibit erroneous strain since the element will have been distorted by the prior activated elements. This strain is subtracted from the current strain when used to compute the stress, so that the initial strain of the activated element is zero. Then, the next element is activated and the process is repeated until all elements are activated. For this model, the thermomechanical deformation (defined in Eq. 7) at the last time step is used to compute the objective function.

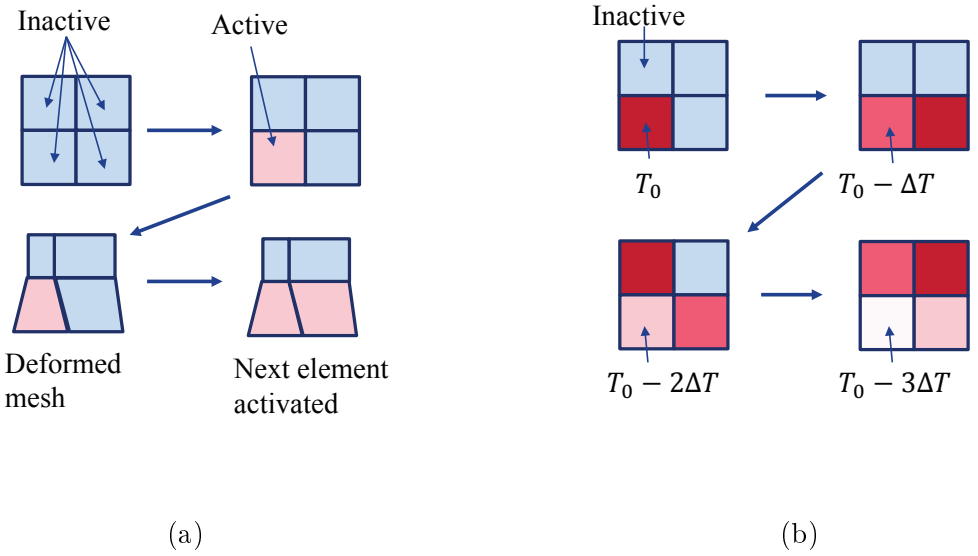

Fig. 1 Schematic of a) the element activation process and b) the element temperature histories

Note that the strain subtraction procedure is an approximation, and a more accurate method would be to reset the initial node positions of the element, recompute the element stiffness matrix, and reassemble the global stiffness matrix. It can be shown that subtracting the strain amounts to a zeroth order approximation of the updated element stiffness matrix; thus, for small displacements this approximation should be sufficient, though error may accumulate during the build process as the upper-most inactive elements deform. However, stress equlibrium and energy conservation are preserved between activation steps.

Approved for public release; distribution is unlimited.

2.4 Compromise Objective Function

The objective function is then a linear combination of the structural problem and the thermomechanical deformation problem, and can be defined as

$$\min_{\boldsymbol{\phi}} f(\boldsymbol{\phi}) = \frac{w}{w_c} c(\boldsymbol{\phi}) + \frac{1-w}{w_d} d_{\text{therm}}(\boldsymbol{\phi}), \tag{9}$$

where $0 \leq w \leq 1$ is the compromise weight and w_c and w_d are normalization factors. Finally, the widely used method of moving asymptotes (MMA) is used as the optimization algorithm.[8]

3. Results

Several results of both optimization processes are given in this section. First, a set of cantilever designs in a square design domain are given while moving the build plate orientation to each edge in the design domain. These results are compared with solutions generated using an overhand constraint approach. In addition, an example using a larger, rectangular design domain is given.

3.1 Square Design Domain

In this section, a square, 1×1 region is used as the design domain and 4 boundary condition configurations are explored, as shown in Fig. 2. In Fig. 2, orange dashed regions indicate the fixed boundary used in the thermomechanical distortion problem (i.e., the build plate), the blue dashed region indicates the fixed boundary for the compliance problem, and the orange arrow indicates the load. For the pure compliance problem, the boundary conditions result in the cantilever solution shown in Fig. 3. The 4 cases then represent placing the thermomechanical boundary condition on each edge of the design domain.

The parameters used in this problem were volume fraction $v_f = 0.5$, Heaviside regularization $\beta = 10$, penalization exponent $p = 4$, compromise weight $w = 0.5$, discretization size 0.02 (50 elements per linear dimension), and filter radius $r_{min} = 0.1$. The optimizer, MMA, was run for 150 iterations. The material properties for all examples were Young's modulus $E = 1$ GPa, Poisson's ratio $\nu = 0.25$, and thermal expansion coefficient $\alpha = 10^{-5}$. Further, the temperature difference for the thermomechanical problem was $\Delta T = -50$ K. Normalization factors w_c and w_d were set to the values of the individual objective functions c and d_{therm} at the initial

Approved for public release; distribution is unlimited.

guess. The optimization results are shown in Fig. 4, and the corresponding objective function values are listed in Table 1. The objective function values in Table 1 show that 2 results are optimal trade-offs (designs b and c) and 2 are dominated (a and d). In other words, the compliance and thermal displacement objective function values of designs a and d are both strictly greater than those of both designs b and c. For designs b and c, design b has lower compliance, but higher thermal displacement than design c; thus, these designs are optimal trade-offs in that neither outperforms the other in terms of both objectives.

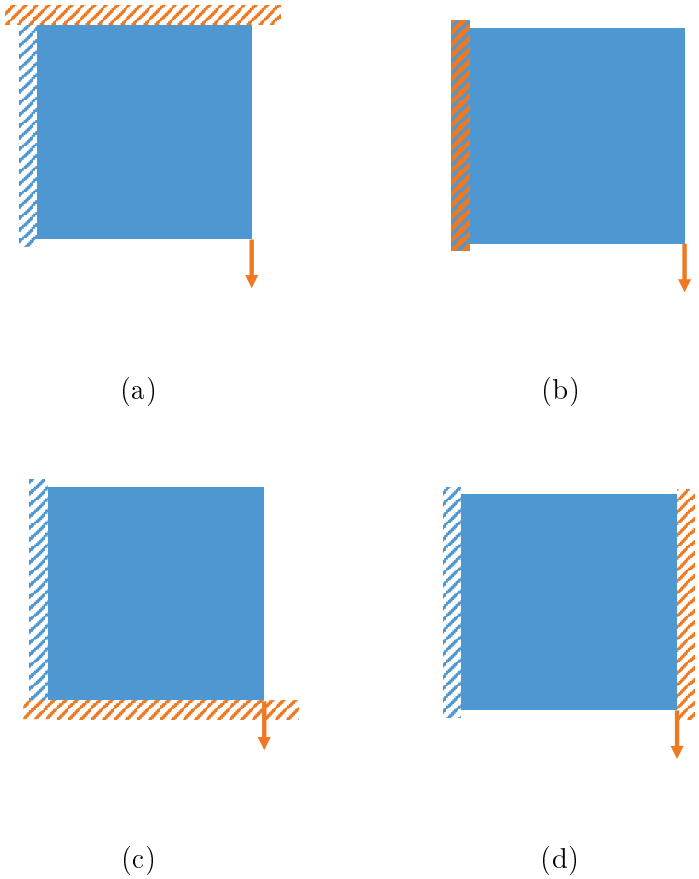

Fig. 2 Schematics of the 4 design cases with a square design domain

Approved for public release; distribution is unlimited.

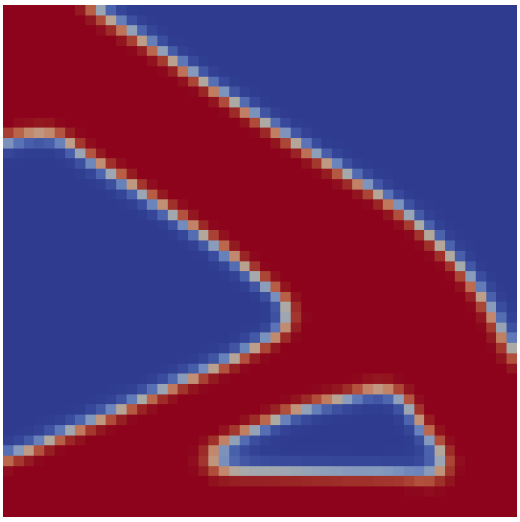

Fig. 3 Static loading solution (i.e., $w = 1$)

Table 1 Objective function values for the four 1×1 design cases

Problem	**Case a**	**Case b**	**Case c**	**Case d**
$\boldsymbol{c}$ **(kNm)**	34.9	25.4	26.6	27.3
$\boldsymbol{d_{\text{therm}}}$ **(µm)**	825	390	236	519

Approved for public release; distribution is unlimited.

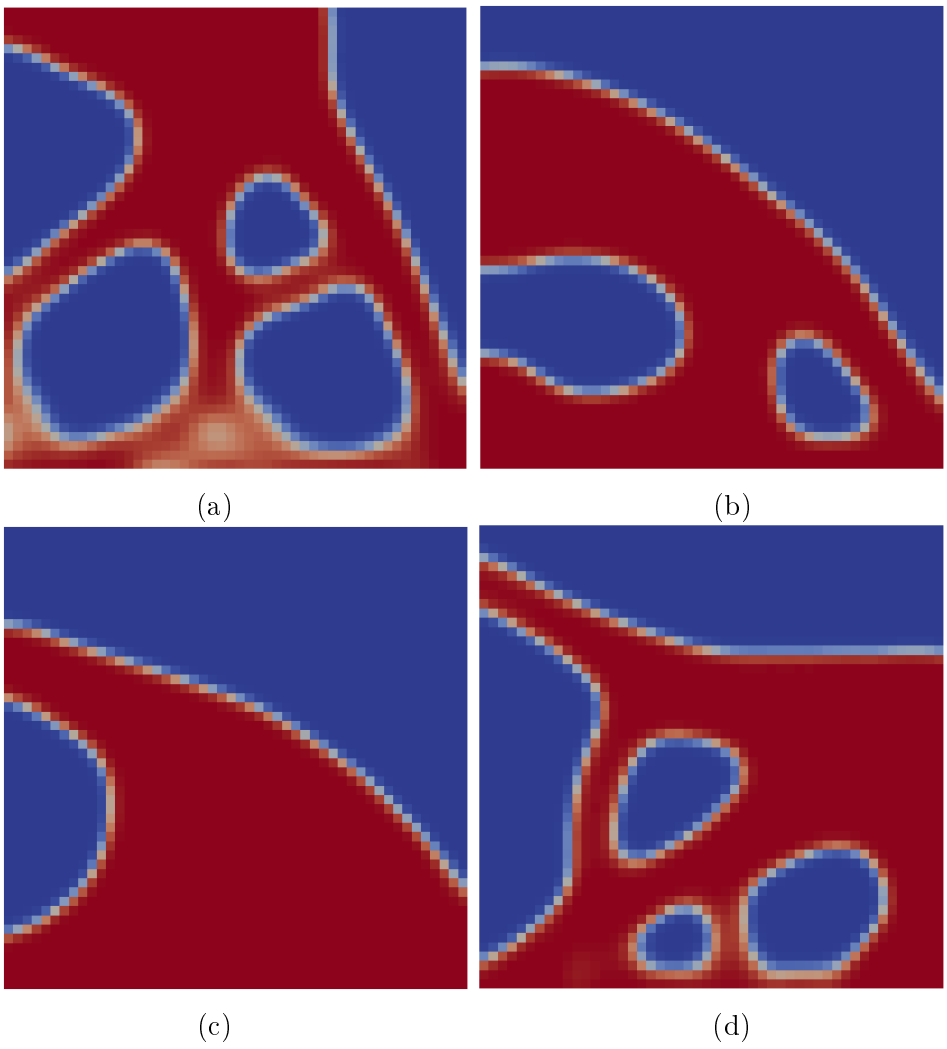

Fig. 4 Results of the 4 design cases

The thermomechanical method discussed here has a similar goal to and may be compared with an overhang constraint approach.[3] The overhang constraint method was applied to the design cases illustrated in Fig. 2 using an overhang angle of $45°$, and the results are shown in Fig. 5. (Note that Fig. 5 also shows a density plot though a different color scheme is used.) Two design cases (b and c) appear fairly similar between the 2 methods, while cases a and d differ more significantly. The advantage of the thermomechanical approach is that the overhang constraint may be overly restrictive for short overhanging sections of a part. In other words, the length of an overhanging section is also important in addition to overhang angle to build success. The overhang constraint approach does not consider the length of a section,

Approved for public release; distribution is unlimited.

while in the thermomechanical approach this may be a natural outcome. Designs b and c may then be similar in both methods because the overhang constraint does not significantly alter the designs when compared with the unconstrained design (see Fig. 3) and so neither does the thermomechanical method. Design cases a and d do differ significantly from the unconstrained design, and so because the thermomechanical method allows for overhanging features, it does result in designs different from the overhang constrained designs.

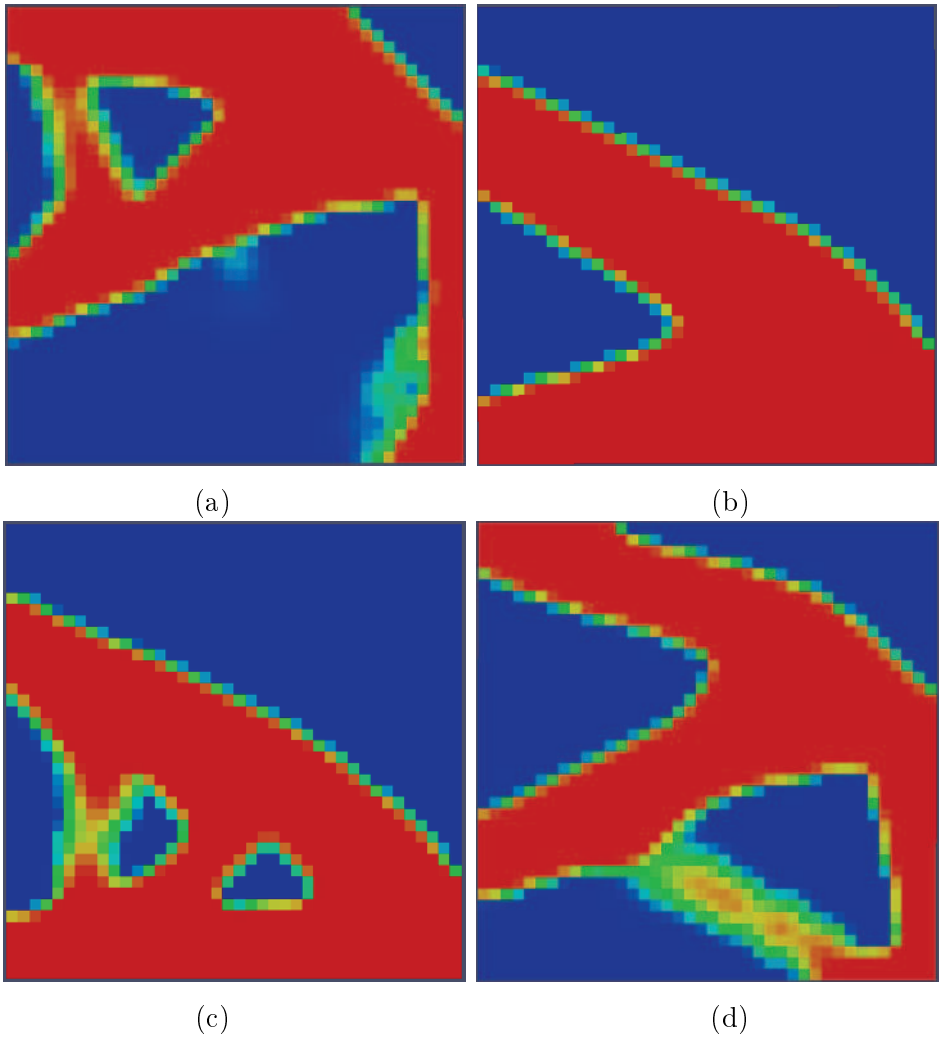

Fig. 5 Results of the 4 design cases using a 45° overhang angle constraint

Figures 6 and 7 show the thermally induced displacement of design cases a and d. In each figure, subfigure a) shows the initial configuration and subfigure b) shows the final configuration after cooling. Note that the displacement is exaggerated by

Approved for public release; distribution is unlimited.

a factor of 1000, and elements with a density of less than 0.25 are removed as the large deformations associated with these elements obscure the results.

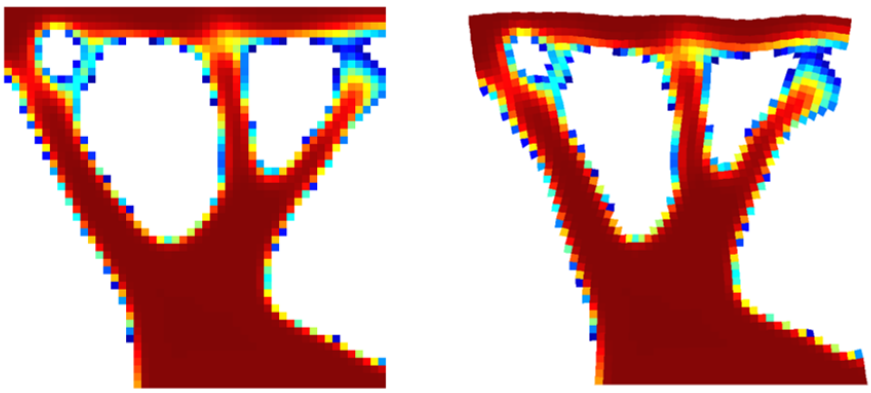

(a) (b)

Fig. 6 Thermal deformation of design case a: a) initial geometry and b) final result

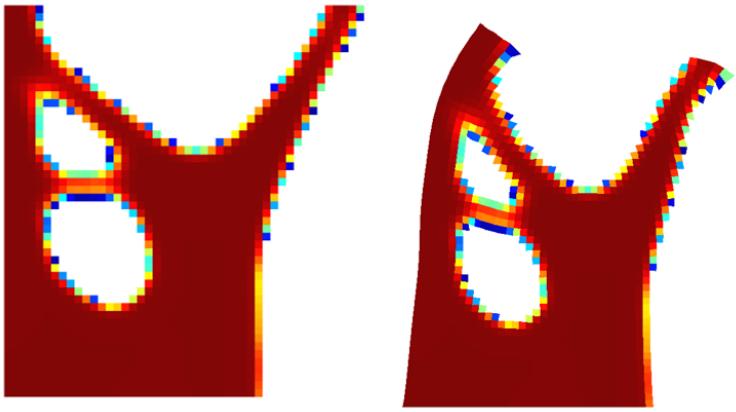

(a) (b)

Fig. 7 Thermal deformation of design case d: a) initial geometry and b) final result

Approved for public release; distribution is unlimited.

To illustrate the effect of varying the compromise weight w, design case d from Fig. 4 was repeated using 8 values of w: 0.1, 0.2, 0.3, 0.4, 0.6, 0.7, 0.8, and 0.9. These results are shown in Fig. 8, where Fig. 8a shows the result for $w = 0.1$, and w increases to a value of 0.9 for Fig. 8h. (Recall that the result in Fig. 4d corresponds to a value of $w = 0.5$.) As can be seen, for lower values of w the results display fewer overhanging features and may represent designs that are less prone to build failures with an additive process. In addition, Fig. 9 shows the individual (penalized) objective function values (c and d_{therm}) with the lowest value of c corresponding to the highest value of w.

Approved for public release; distribution is unlimited.

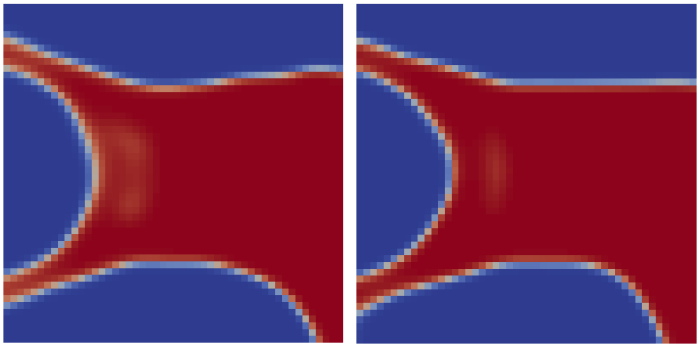

(a) $w = 0.1$ (b) $w = 0.2$

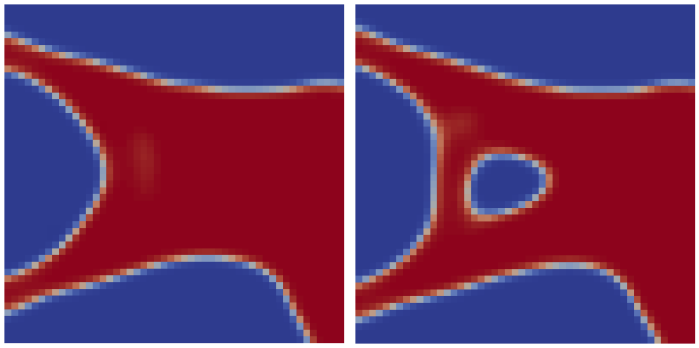

(c) $w = 0.3$ (d) $w = 0.4$

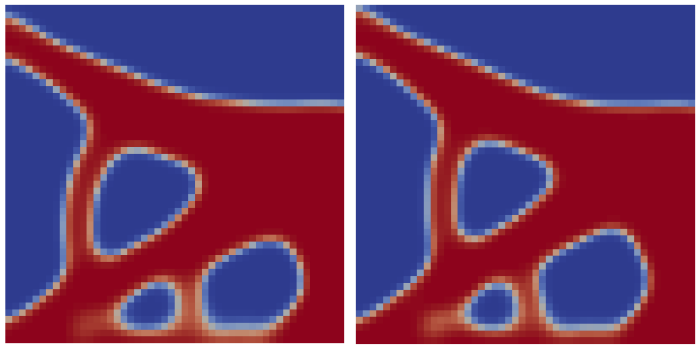

(e) $w = 0.5$ (f) $w = 0.6$

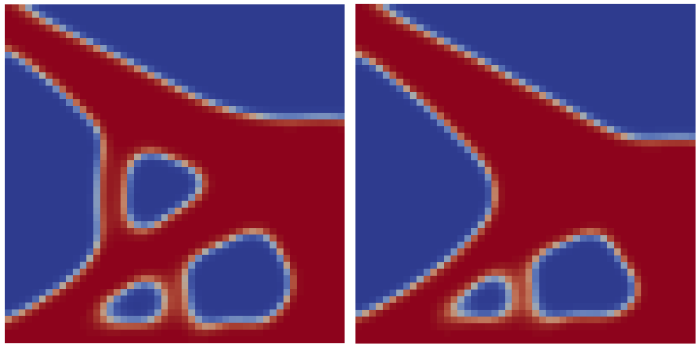

(g) $w = 0.7$ (h) $w = 0.8$

Fig. 8 Results of design case 4 with varying w

Approved for public release; distribution is unlimited.

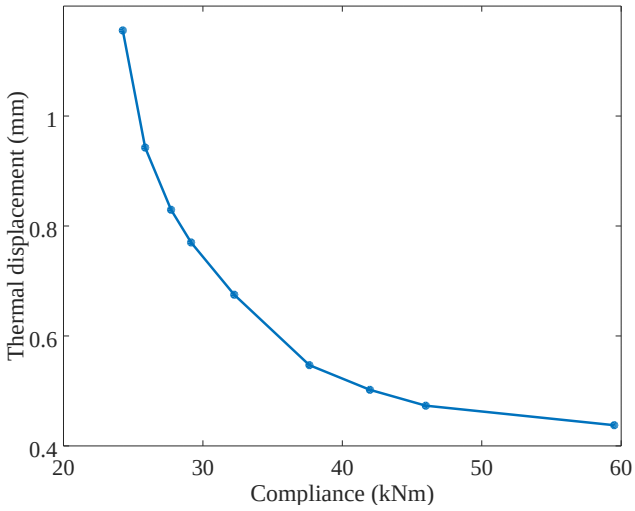

Fig. 9 Individual objective function values for varying w in Fig. 4

Finally, design case b was repeated using the element-birth model. In this example, the discretization size was reduced to 30 elements per linear dimension, and the stiffness penalization exponent was increased to $p_1 = 6$. The size of the added material at each step was 0.1-by-0.1, or 3 elements, and the temperature was decreased for each active element by 0.5 K. Optimization results are shown for compromise weight $w = 0.9$ and $w = 0.95$ in Fig. 10 along with the pure compliance result ($w = 1$) for comparison.

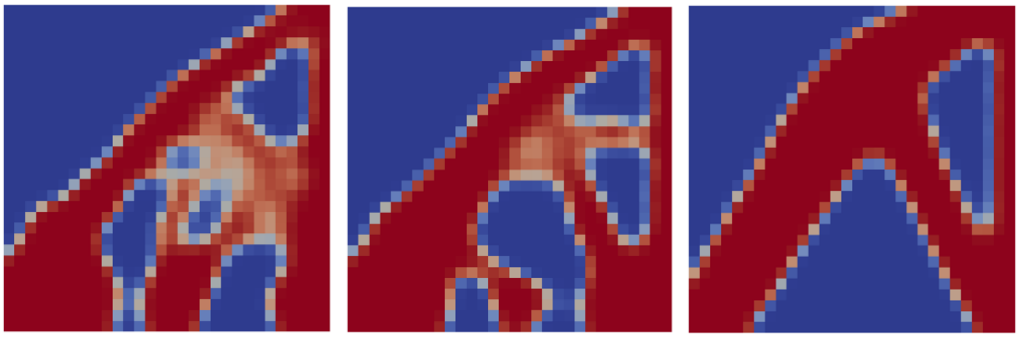

(a) $w = 0.9$ (b) $w = 0.95$ (c) $w = 1$

Fig. 10 Results of the element-birth model with varying w

Approved for public release; distribution is unlimited.

3.2 6×1 Design Domain

In this example, a 6×1 design domain was used with half-symmetry boundary conditions. The bottom corners were fixed, and load was applied to the top center. Parameters for the optimization algorithm and discretization were identical to those of the 1×1 design cases. First, the thermomechanical fixed boundary was placed on the bottom edge of the domain, resulting in the design shown in Fig. 11a. Also shown in Fig. 11b is the same compliance problem optimized with an overhang angle constraint of $45°$. It is apparent from Fig. 11 that the thermomechanical result still exhibits overhanging features, though note that overhanging features may not lead to a failed build because the length of those features is important. The individual objective function values for the thermomechanical optimization were $c = 4242.17\ \mathrm{N\,m}$ and $d_{\text{therm}} = 59.2\ \mu\mathrm{m}$.

Finally, the problem was repeated with the thermomechanical fixed boundary on the top edge of the region. This result is shown in Fig. 12 (also compared with an overhang constrained design) and had individual objective function values of $c = 4712\ \mathrm{N\,m}$ and $d_{\text{therm}} = 76.8\ \mu\mathrm{m}$. In this case, building from the top down is clearly suboptimal as both the compliance and thermal displacement are higher.

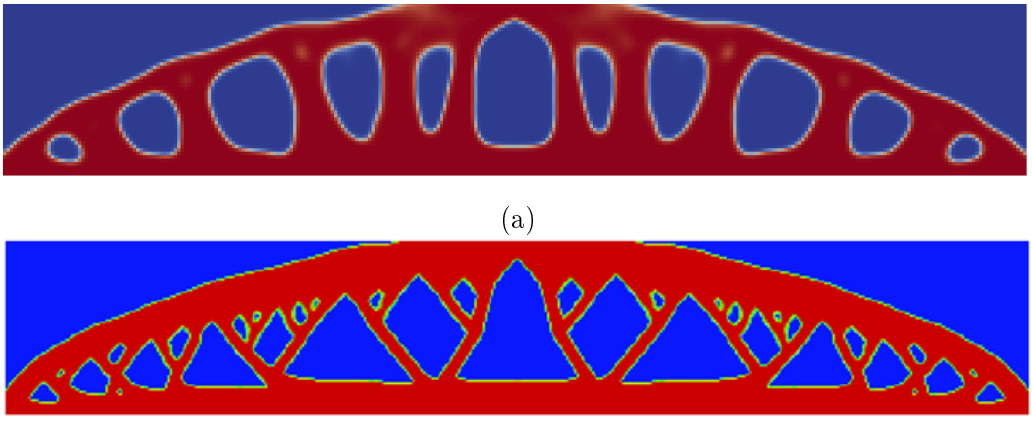

(a)

(b)

Fig. 11 Results of the 6×1 design domain using a) the thermomechanical model and b) a $45°$ overhang constraint

Approved for public release; distribution is unlimited.

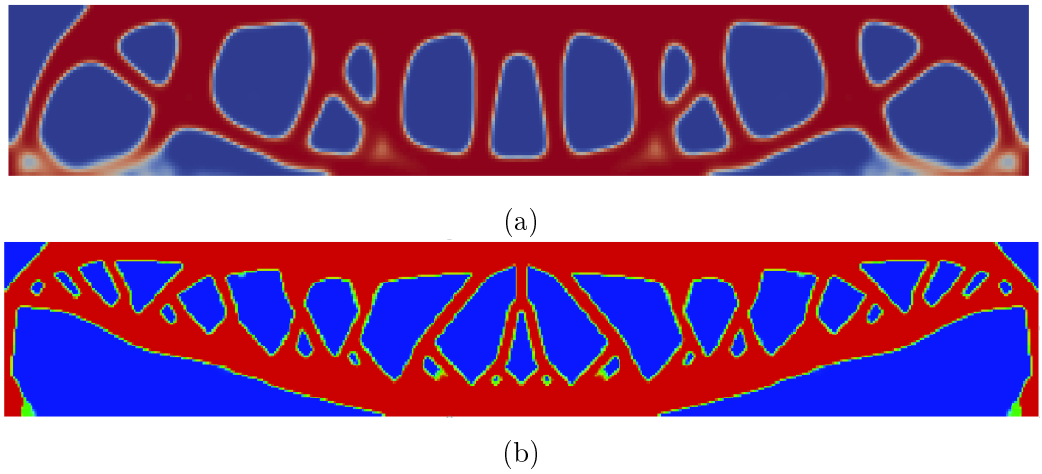

(a)

(b)

Fig. 12 Results of the 6×1 design domain (with the build plate placed on the top edge) using a) the thermomechanical model and b) a 45° overhang constraint

3.3 Comparison

Because the element-birth approach is much more computationally expensive than the basic thermomechanical model, it is worthwhile to compare the results of the approaches directly. If the basic thermomechanical optimization approach yields results that are near-optimal using the element-birth model, we may use the cheaper optimization result as an initial guess for the more expensive, hopefully saving computation time.

To that end, the basic thermomechanical model was optimized using the same discretization as the element-birth model, and the results are shown in Fig. 13. After optimization, the thermal distortion objective (d_{therm}) of the basic result was evaluated using the element-birth model. In this case, the unpenalized thermal distortion was 1.78×10^{-4} for the element-birth result and 2.14×10^{-4} for the basic thermomechanical result, which is about a 20% difference.

3.4 3-D Results

Finally, the basic thermomechanical model was used in 3-D in a $1 \times 0.5 \times 0.5$ region in a cantilever-like loading with a volume fraction of $v_f = 0.3$. The fixed boundary was located on the $x = 0$ plane, and the load was $-y$-directed and located at the point $(1, 0, 0.5)$. Two build directions, x and y—meaning that the build plates were located on the $x = 0$ and $y = 0$ planes, respectively—were tested using a weight of

Approved for public release; distribution is unlimited.

$w = 0.5$. The results of the optimization are shown in Fig. 14 with the pure compliance ($w = 0$) result shown in Fig. 14(a) for comparison. The compliance of each result was 35.4, 40.8, and 43.4 kNm for the pure compliance, x build direction, and y build direction results, respectively. Comparing the thermal displacement between the 2 build directions is not informative because the surface area of the build plates is different; however, comparing the thermal displacement of the pure compliance problem with each reveals that each result is a trade-off with the pure compliance result, as expected. Table 2 lists the objective function values for each result.

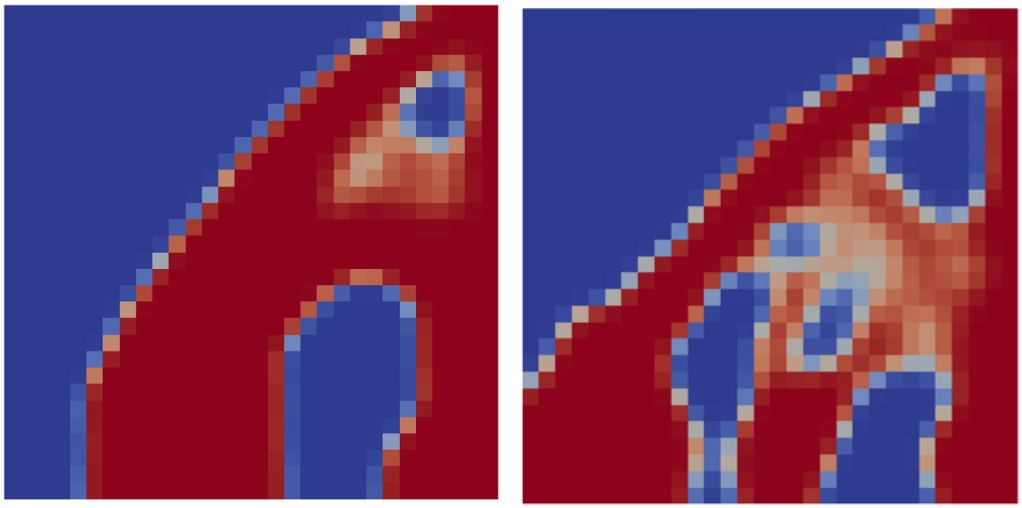

(a) (b)

Fig. 13 Comparison of a) basic and b) element-birth thermomechanical optimization problems

Table 2 Objective function values for the 3-D design cases

Problem	**Pure compliance**	**x-directed build**	**y-directed build**
c (kNm)	35.4	40.8	43.4
x-directed d_{therm} (μm)	593	411	652
y-directed d_{therm} (μm)	443	380	238

Approved for public release; distribution is unlimited.

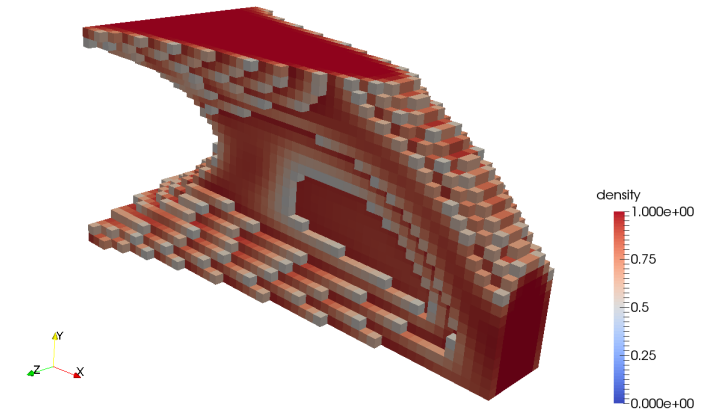

(a)

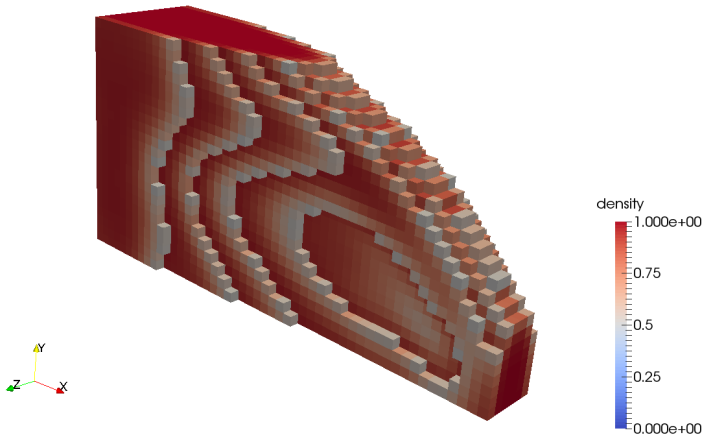

(b)

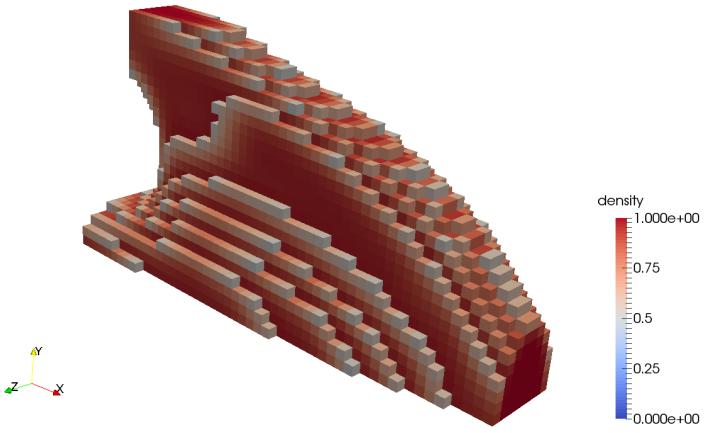

(c)

Fig. 14 Results for the $1\times0.5\times0.5$ design domain with a) no thermomechanical model ($w=1$), b) build direction in the x-direction and, c) build direction in the y-direction

Approved for public release; distribution is unlimited.

4. Conclusions

An optimization technique was presented that pairs a minimum compliance problem with surrogate models for the AM process. The goal was to minimize thermal distortions induced during the build process to generate more readily manufacturable designs. Two process models were used, the first being a one-step thermomechanical simulation in which the entire part begins at the same initial temperature and cools at the same rate. The second was an element-birth iterative model, in which elements are activated in turn and at a given initial temperature. At each step, activated elements are cooled at a linear rate. For the optimization formulation, an HPM and SIMP penalization were used as the topology parameterization, and the MMA algorithm was used as the optimizer. Finite differences were used to compute the gradient of the topology representation.

Results demonstrate the viability of the method, and several examples were presented with different design domains. Further, the results were compared with overhang angle constrained results, demonstrating some similarities and differences between the methods. Finally, the basic thermomechanical model was compared with the element-birth model demonstrating that the 2 methods do give different optimization results, even though they use the same objective function. The difference in the thermal displacement objective function value for the same design case was found to be approximately 20%. While this is a rather large difference, the cheaper model may be used for an initial guess for the more expensive model, as the element-birth model is significantly more computationally expensive for a full optimization run. Consider, the computational complexity of a naïve implementation of the basic model is $O(N^4)$ at worst when using a finite difference-based gradient computation because a matrix equation must be solved for each element in the mesh. For the element-birth model, the complexity grows to $O(N^5)$ because each step of the element-birth process involves solving a new matrix equation, which must be done for each element again to compute the gradient. Regardless of the matrix equation solution technique (which may reduce the computational complexity), the element birth model will always have a computational complexity of one power higher. Additional efficiency may of course be gained by using an adjoint gradient approach for the basic thermomechanical model, though it remains to be seen if an adjoint can be formulated for the element-birth model. In the future, the

Approved for public release; distribution is unlimited.

designs generated with both approaches will be tested using a suitable AM technique to determine buildability.

Using the concept of pairing a process model with the optimization problem, there are several other options that may yield better results and will be explored in the future. First, residual stress minimization could be used rather than displacement minimization. Second, build failures often occur because the built part warps to such a degree that it is impacted by the recoater blade or roller. A constraint could then be placed on the maximum allowable thermal deformation seen in any single build layer.

Approved for public release; distribution is unlimited.

5. References

1. Guest JK, Prévost JH, Belytschko T. Achieving minimum length scale in topology optimization using nodal design variables and projection functions. International Journal for Numerical Methods in Engineering. 2004;61(2):238–254.

2. Kranz J, Herzog D, Emmelmann C. Design guidelines for laser additive manufacturing of lightweight structures in tial6v4. Journal of Laser Applications. 2015;27(S1):S14001.

3. Gaynor AT, Guest JK. Topology optimization considering overhang constraints: eliminating sacrificial support material in additive manufacturing through design. Structural and Multidisciplinary Optimization. 2016;54(5):1157–1172.

4. Sigmund O, Petersson J. Numerical instabilities in topology optimization: a survey on procedures dealing with checkerboards, mesh-dependencies and local minima. Structural Optimization. 1998;16(1):68–75.

5. Bendsøe M. Optimal shape design as a material distribution problem. Structural Optimization. 1989;1(4):193–202.

6. Zhou M, Rozvany G. The COC algorithm, part II: topological, geometrical and generalized shape optimization. Computer Methods in Applied Mechanics and Engineering. 1991;89(1-3):309–336.

7. Zhang W, Yang J, Yingjie X, Gao T. Topology optimization of thermoelastic structures: mean compliance minimization or elastic strain minimization. Structural and Multidisciplinary Optimization. 2013;49:417–429.

8. Svanberg K. The method of moving asymptotes: a new method for structural optimization. International Journal for Numerical Methods in Engineering. 1987;24(2):359–373.

Approved for public release; distribution is unlimited.

List of Symbols, Abbreviations, and Acronyms

2-D	2-dimensional
3-D	3-dimensional
AM	additive manufacturing
FE	finite element
HPM	Heaviside projection method
MMA	method of moving asymptotes
SIMP	solid isotropic material with penalization

Approved for public release; distribution is unlimited.

1 (PDF)	DEFENSE TECHNICAL INFORMATION CTR DTIC OCA
2 (PDF)	DIR ARL IMAL HRA RECORDS MGMT RDRL DCL TECH LIB
1 (PDF)	GOVT PRINTG OFC A MALHOTRA
80 (PDF)	RDRL CIH C E CHIN D GROVE J KNAP M LEE RDRL SE W BENARD RDRL-SED-P M BERMAN L BOTELER RDRL WM B FORCH S KARNA J LA SCALA A RAWLETT S SCHOENFELD J ZABINSKI RDRL WML A B BREECH RDRL WML B I BATYREV J BRENNAN E BYRD S IZVYEKOV J LARENTZOS W MATTSON B RICE D TAYLOR N WEINGARTEN RDRL WML G J O′GRADY RDRL WML H B AYDELOTTE C MEYER D SCHEFFLER B SCHUSTER RDRL WMM J BEATTY R DOWDING M VANLANDINGHAM RDRL WMM A D BAECHLE D O′BRIEN J TZENG C YEN RDRL WMM B B AKSOYLU C DECKER C FOUNTZOULAS A GAYNOR G GAZONAS E HERNANDEZ D HOPKINS

B LOVE
B POWERS
T SANO
M TSCHOPP
T WALTER
R WILDMAN
RDRL WMM D
R BRENNAN
B MCWILLIAMS
S WALSH
J YU
RDRL WMM E
J LASALVIA
J SWAB
D SHREIBER
RDRL WMM G
J ANDZELM
J LENHART
K MASSER
C RINDERSPACHER
T SIRK
Y SLIOZBERG
RDRL WMP
D LYON
RDRL WMP A
S BILYK
J CAZAMIAS
RDRL WMP B
S SATAPATHY
M SCHEIDLER
T WEERASOORIYA
RDRL WMP C
M FERMEN-COKER
M GREENFIELD
B LEAVY
J LLOYD
C MEREDITH
S SEGLETES
A SOKOLOW
C WILLIAMS
RDRL WMP D
R DONEY
C RANDOW
S SCHRAML
M ZELLNER
RDRL WMP E
T JONES

Approved for public release; distribution is unlimited.

INTENTIONALLY LEFT BLANK.